



MODELING SLIP, KINK AND SHEAR BANDING IN CLASSICAL AND GENERALIZED SINGLE CRYSTAL PLASTICITY

S. FOREST

Ecole des Mines de Paris/CNRS, Centre des Matériaux, URA 866, BP 87, 91003 Evry, France

(Received 27 October 1997; accepted in revised form 20 November 1997)

Abstract—Classical crystal plasticity can account for slip, kink and shear band formation in metal single crystals exhibiting a softening behavior. In the case of multiple slip, the stability of symmetric multi-slip configurations depending on the self/latent hardening ratio is investigated. Finite element simulations of symmetric and symmetry-breaking localization modes in single crystals oriented for double slip in tension are presented. Some shortcomings of classical crystal plasticity are then pointed out that can be solved using a Cosserat crystal plasticity model that explicitly takes elastoplastic lattice torsion-curvature into account. The classical theory predicts for instance the same critical hardening modulus for the onset of slip and kink banding. This is not the case any more in generalized crystal plasticity, as shown by a bifurcation analysis and finite element simulations of Cosserat crystals. © 1998 Acta Metallurgica Inc.

Résumé—La théorie classique de la plasticité cristalline permet de rendre compte de la formation de bandes de glissement, de bandes en genou et de bandes de cisaillement dans les monocristaux métalliques. Dans le cas du glissement multiple, on étudie la stabilité des configurations de glissement multiple symétrique en fonction du rapport entre autoécrouissage et écrouissage latent. On présente des simulations par éléments finis de modes de localisation symétriques et avec brisure de symétrie. Quelques insuffisances de la théorie classique sont ensuite mises en évidence. Pour y remédier, une théorie de Cosserat du monocristal est présentée, qui prend explicitement en compte la courbure-torsion plastique du réseau. En particulier, la théorie classique prédit le même seuil d'apparition pour les bandes de glissement que pour les bandes en genou. Ce n'est plus le cas dans le cadre de la plasticité cristalline généralisée, ainsi que le montrent une analyse de bifurcation et des simulations par éléments finis avec le modèle de Cosserat. © 1998 Acta Metallurgica Inc.

Zusammenfassung—Die Bildung von Gleit-, *kink* und Scherbandern in Einkristallen kann von der klassischen Kristallplastizität vorhergesagt werden. Im Falle mehrerer gleichzeitig aktivierter Gleitsysteme wird die Stabilität solcher Konfigurationen in Abhängigkeit von Selbst/latenter Verfestigung untersucht. FE Simulationen von symmetrischen und Symmetrie-brechenden Lokalisierungsmoden werden durchgeführt. Ein paar Unzulänglichkeiten der klassischen Kristallplastizität werden erwähnt, die durch die Entwicklung einer Cosserat Theorie der Kristallplastizität gelöst werden. Dabei wird die elastoplastische Krümmung des Gitters explizit berücksichtigt. Die klassische Theorie gibt den gleichen kritischen Verfestigungsmodul für die Bildung von Gleit- und *kink* Bändern. Das ist nicht mehr der Fall im Rahmen der generalisierten Theorie, was durch eine Bifurkationsanalyse und FE Simulationen von Cosserat-Kristallen gezeigt wird. © 1998 Acta Metallurgica Inc.

1. INTRODUCTION

1.1. Heterogeneous nature of slip

In the endeavour to connect microscopic physical mechanisms and the macroscopic mechanical behavior of metal crystals, one of the main difficulties to be overcome arises directly from the intrinsically heterogeneous nature of slip: deformation of crystalline solids occurs by the development of discrete slip steps visible sometimes by the necked eye. Neuhäuser [1] gives a very precise typology of these discrete phenomena, that take place at various length scales. A *glide band* is a cluster of surface steps resulting from single or few dislocations on closely spaced neighbouring planes. This gives rise to a rather homogeneous deformation of the speci-

men. In contrast a *slip band* is a cluster of some sharp offsets corresponding to the emergence of many dislocations on a few close crystallographic planes. Often the slip bands are again clustered in units called *slip band bundles*. The size of these plastic discrete patterns ranges from tens of Å for slip lines to about 1 mm for slip band bundles or Piobert–Lüders bands.

Mader [2] reports a homogeneous distribution of slip bands in aluminium single crystals during stage I. During stage II slip line bundles form and the deformation becomes heterogeneous. Slip lines of the secondary systems are observed. Intense shear bands and some kink bands appear at stage III while traces of cross-slip are observed. Kink bands are also reported in Ref. [3]: they are perpendicular

to the glide direction. Similar deformation modes are observed in copper for different temperatures. Kink bands are also mentioned by Jaoul [4] and Friedel [5]. Mader and Seeger [3] consider that kink bands are not spurious effects but the natural result of some dislocation motion. Within kink bands slip occurs on the primary system but the secondary system can also be activated. Secondary slip in kink bands has also been noted in Ref. [6] after 4% of deformation in aluminium crystals. They remark that no kink bands are observed in crystals oriented for polyslip. Kink bands will be precisely defined in the Section 1.2. If multiple slip occurs inside a localization band, the more general term shear band will be used.

1.2. Localized bifurcation modes in elastoplasticity

Since Asaro and Rice [7], the occurrence of shear bands in single crystals has been described by a bifurcation analysis of the set of constitutive equations.

Ideally, localized deformation bands are bounded by two parallel surfaces S across which the velocity gradient $\dot{\mathbf{u}} \otimes \bar{\mathbf{v}}$ and the stress rate $\dot{\boldsymbol{\sigma}}$ are discontinuous. However, Hadamard's compatibility conditions and equilibrium at the interfaces imply:

$$\exists \bar{\mathbf{g}} / [\dot{\mathbf{u}} \otimes \bar{\mathbf{v}}] = \bar{\mathbf{g}} \otimes \bar{\mathbf{n}} \quad (1)$$

$$[[\dot{\boldsymbol{\sigma}}]] = \bar{\mathbf{n}} = 0 \quad (2)$$

where $\bar{\mathbf{n}}$ is the normal to S and the brackets denote a jump. In the case of elastoplasticity at small strains, the constitutive equations take the multi-branch incremental form:

$$\dot{\boldsymbol{\sigma}} = \mathbf{L} : \dot{\boldsymbol{\varepsilon}} \quad (3)$$

where $\boldsymbol{\varepsilon}$ is the strain tensor and \mathbf{L} the four rank tensor of the tangent moduli. Equations (1) and (2) lead to the relationship

$$\tilde{\mathbf{Q}} \bar{\mathbf{g}} = 0 \quad (4)$$

where $Q_{ij} = n_k L_{iklj} n_l$ is the acoustic tensor. The solution can be non-trivial when the acoustic tensor becomes singular. It can be shown that there is an equivalence between the *loss of ellipticity* of the governing equations and the existence of discontinuous bifurcation modes [15]. The control parameter of such a bifurcation analysis in isotropic elastoplasticity usually is the hardening modulus H , \mathbf{L} being a function of H .

Asaro and Rice [7] performed such a bifurcation analysis at large strains for elastoplastic single crystals undergoing single slip. They found two possible localization modes: slip and kink bands. For slip bands, the localization plane coincides with the glide plane of normal $\bar{\mathbf{z}}$ of the considered slip system. In the case of kink bands, the localization plane is normal to the slip direction $\bar{\mathbf{m}}$. These two localization modes simultaneously become possible

for a critical hardening modulus H^{cr} which is slightly positive in the analysis at large strains. If only localization at incipient plasticity is considered, $H^{cr} = 0$. Under such circumstances, strain softening is required for localized bifurcation modes to occur.

1.3. Local softening mechanisms

Estrin and Kubin [8] have investigated averaged properties of dislocations over a local volume in order to calculate a local strain hardening. They proposed a system of differential equations accounting for the evolution of densities of mobile and forest dislocations including production, annihilation and interaction terms. Solving this differential system yields the evolution of local strain hardening H as a function of axial deformation ε . The competition of hardening and softening terms gives rise to three distinct domains. In the first domain, H turns out to be negative. In the intermediate domain, the material hardens because the forest density is far from saturation while the density of mobile dislocations stabilizes. Lastly, strain hardening decreases under the influence of dynamic recovery.

Then a bifurcation analysis based on the study of possible growth of local fluctuations, shows that the stability domain of uniform deformation is contained in (though smaller than) the region of positive hardening rate. In the first domain, uniform slip is unstable. It is suggested that this behaviour is typical of the occurrence of individual slip lines or slip bands. In contrast the instability reached at the end of the third domain for large deformations will lead to non-uniform deformation like necking or shear banding. Thus, plastic deformation will necessarily start in a non-uniform fashion.

Resorting to dislocation dynamics, Canova *et al.* [9] have simulated the mechanisms by which precipitate shearing or the destruction of short range order lead to glide softening and strain localization.

1.4. Scope of this work

This explains why, in Section 2, material softening is introduced in the constitutive behavior of single crystals in order to trigger slip band formation in classical crystal plasticity. The case of multiple slip is tackled in Section 3 where the stress is laid on the influence of latent hardening or softening on the stability of multiple slip configurations.

After these analyses within the framework of classical crystal plasticity, some shortcomings are pointed out that indicate the necessity of enriching the description of dislocation populations in the continuum approach. This is then done within the framework of a Cosserat theory. A complete set of kinematic and constitutive equations is presented. The bifurcation analysis must be carried out again for the Cosserat crystal. This will be done in the case of single slip. It will appear that the proposed theory separates the onsets of the localization

modes slip/kink bands that are identical in the classical case.

For the sake of brevity and because localization phenomena occurring at incipient plasticity is dealt with, the classical and Cosserat theories are presented in the case of small deformations. However, most computations of Sections 2 and 3 have been performed also using a large strain formulation and this does not affect significantly the presented results.

The numerical simulations presented in this work have been performed using the inhouse object-oriented finite element program ZéBuLoN [10]. The local integration of the constitutive equations is performed using a second order Runge–Kutta method and, for the global resolution, it is resorted to a BFGS method. The element used are 20-node bricks with full or reduced integration (27 or 8 Gauss points).

2. SINGLE SLIP LOCALIZATION MODES

In this section, after recalling the general setting, the simulation of localization modes in single crystals undergoing single slip in tension is focused on.

2.1. General case

In single crystals, the plastic strain rate is the sum of the contributions of n slip systems

$$\dot{\boldsymbol{\varepsilon}}^p = \sum_{s=1}^n \dot{\gamma}^s \{\tilde{\mathbf{P}}^s\} \quad (5)$$

where $\tilde{\mathbf{P}}^s = \bar{\mathbf{m}}^s \otimes \bar{\mathbf{z}}^s$ is the orientation tensor of system s , dyadic product of the glide vector $\bar{\mathbf{m}}^s$ and the normal to the slip plane $\bar{\mathbf{z}}^s$. The brackets represent the symmetric part. Schmid's law written for each slip system gives a yield surface with vertexes:

$$\tau^s - r^s = 0 \quad (6)$$

where $\tau^s = \tilde{\boldsymbol{\sigma}} : \tilde{\mathbf{P}}^s$ is the resolved shear stress on slip system s . Mandel's hardening rule [11] involves an interaction matrix to describe self- and latent hardening:

$$\dot{\gamma}^s = \sum_{g=1}^n H^{sg} \dot{\gamma}^g \quad \text{with } \dot{\gamma}^s = |\dot{\gamma}^s|. \quad (7)$$

In the particular case of single crystals in tension undergoing symmetric multiple slip on n systems and assuming a diagonal or isotropic interaction matrix, the previous expressions simplify and the

expression of the elastoplastic tangent moduli reads

$$\mathbf{L} = \mathbf{E} - \frac{(\mathbf{E} : \tilde{\mathbf{P}}) \otimes (\tilde{\mathbf{P}} : \mathbf{E})}{H + \tilde{\mathbf{P}} : \mathbf{E} : \tilde{\mathbf{P}}} \quad (8)$$

where \mathbf{E} is the four-rank elasticity tensor, $\tilde{\mathbf{P}}$ is the sum of the $\tilde{\mathbf{P}}^s$ of the activated slip systems (see Ref. [13] for the expression of H). A bifurcation analysis has been performed in Ref. [13]. The main results are recalled in Table 1, that gives in each case the orientation of the first possible localization band and the associated critical hardening modulus. In the case of single slip, the results are the same as in Ref. [7]: slip and kink bands can form simultaneously as soon as the hardening modulus vanishes.

2.2. Slip and kink banding in a tube

As an introduction to the FE simulations of strain localization in single crystals, the formation of a slip and a kink band in a f.c.c. single crystal tube oriented for single slip in tension is first presented. The material exhibits a short strain-hardening period followed by strain-softening. A material defect (a slightly smaller initial critical resolved shear stress) is introduced in one element to trigger localization. The following non-linear hardening law is used instead of equation (7):

$$r^s = r_0^s + q_1 \sum_{r=1}^n h^{sr} (1 - \exp(-b_1 v^r)) + q_2 (1 - \exp(-b_2 v^s)) \quad (9)$$

r_0 denoting the initial threshold. The illustrative material parameters in the simulation are:

$$\begin{aligned} E &= 200000 \text{ MPa}, & \nu &= 0.3, \\ r_0 &= 50 \text{ MPa}, & q_1 &= -45 \text{ MPa}, \\ b_1 &= 210, & q_2 &= 22 \text{ MPa}, \\ b_2 &= 900. \end{aligned} \quad (10)$$

The interaction matrix h^{sr} does not play any role in this section since only single slip will take place. It will become important in Section 3. The tube axis coincides with a [123] direction.

The displacement in the initial axis direction only is prescribed at the upper end. Two bands are shown to form in Fig. 1. On the developed surface of the specimen (Fig. 2), it is found that the localization zones coincide with the traces of the slip and kink planes. Such a developed surface can be obtained experimentally using a polymer film

Table 1. Summary of the results of the bifurcation analysis for single crystals in tension oriented for single and symmetric multiple slip (after Ref. [13])

Typical tensile direction	No. of active slip systems, N	Bifurcation planes	Critical hardening modulus
[123]	1	slip plane kink plane	$H = 0$
[012]	2	non-crystallographic	$H \ll 0$
[011]	4	non-crystallographic	$H = 0$
[111]	6	non-crystallographic	$H \ll 0$
[001]	8	non-crystallographic	$H \ll 0$

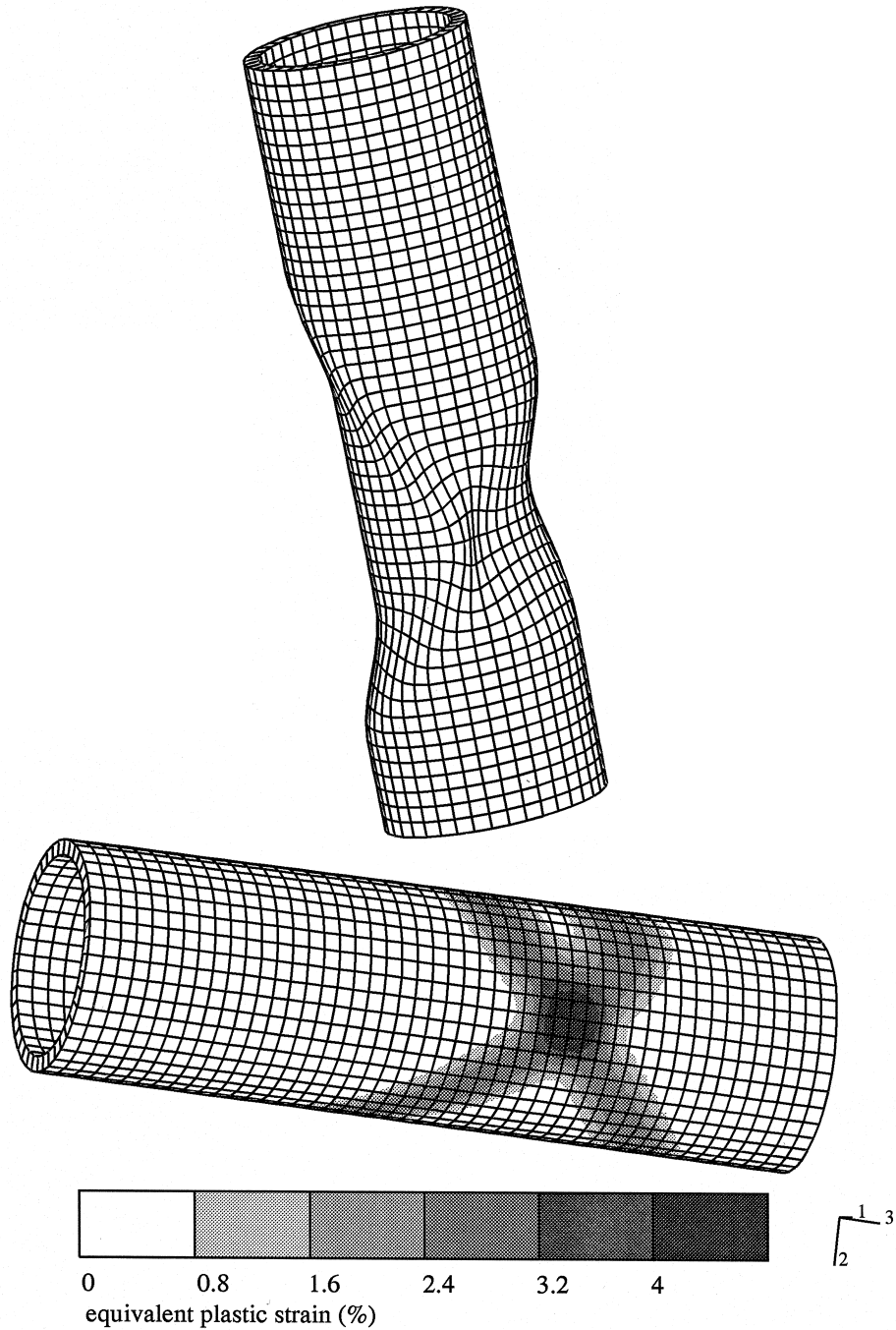


Fig. 1. Slip and kink band formation in a single crystal tube in tension.

deposited on the specimen (Fig. 3, after Ref. [14]): Such sinus curves can be seen but no kink band is reported in Ref. [14] (for various crystal orientations).

2.3. Mesh dependence issue

The emergence of discontinuous bifurcation modes is associated with the loss of ellipticity of the governing equations. The FE simulation of localization in the classical framework then displays spur-

ious mesh-dependence. This is of course the case for the previous results for which slip, kink and shear bands always have the thickness of one element. As pointed out in Ref. [13], the introduction of viscosity as in Section 3 may alleviate the previous statement. This has already been done in Ref. [16]. However the problem would be strictly regularized only in the dynamic case, which is not done here.

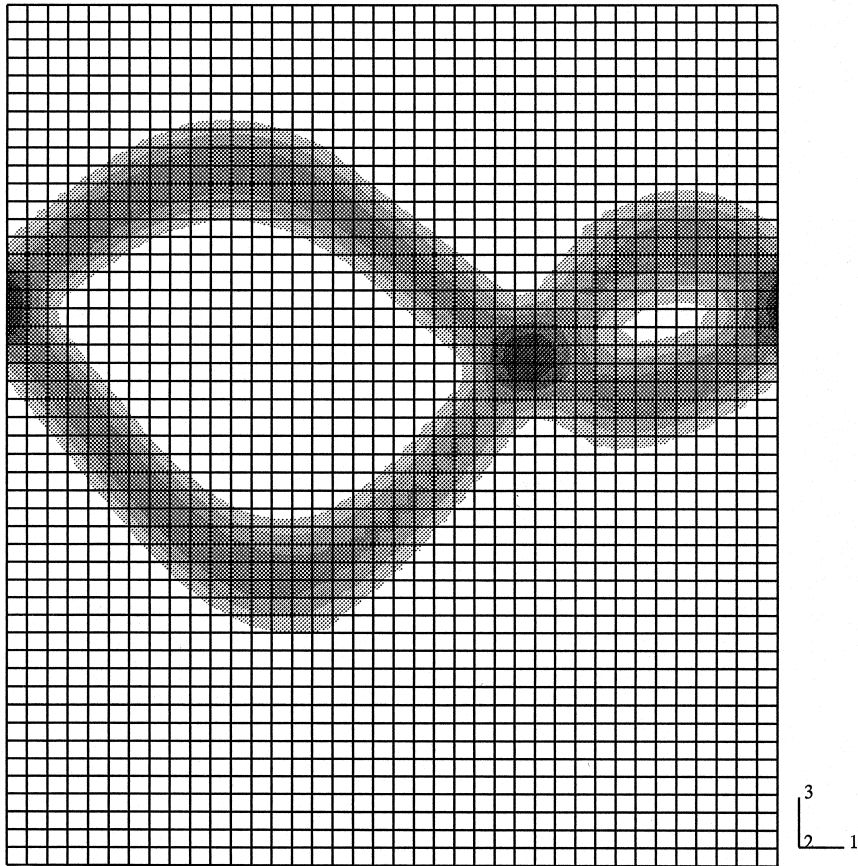


Fig. 2. Developed surface of the tube of Fig. 1 (same deformation scale as in Fig. 1).

Nevertheless the orientation of the band and the type of obtained bifurcation modes are mesh-independent, at least if quadratic elements are used and this is the main issue in this article. An *ad hoc* regularization of the considered localization modes is not the purpose of this work but rather it is the physical relevance of such modes predicted by classical or generalized crystal plasticity theories.

3. MULTIPLE SLIP LOCALIZATION AND LATENT HARDENING

In Ref. [13], multislip configurations that are expected in tension along given directions have been considered, when the interaction matrix is isotropic or diagonal. However, Franciosi *et al.* [17] have shown that pronounced latent hardening makes the simultaneous macroscopic activation of many slip systems locally very unlikely. The predicted slip systems are observed later at larger strains. The interaction matrix cannot then be isotropic at the beginning of plastic flow.

3.1. A simple analysis

In the case of multiple slip and to avoid any indeterminacy of slip activation, an elastoviscoplastic formulation of crystal plasticity with threshold is

adopted:

$$\dot{\gamma}^s = \left\langle \frac{|\tau^s| - r^s}{k} \right\rangle^n \text{sign } \tau^s \quad (11)$$

where k and n are viscosity parameters. The quantity in brackets must be positive for the slip rate to be non-zero.

The bifurcation analysis in Ref. [13] for multislip has provided bifurcation modes for which symmetric slip still occurs inside the band, i.e. the amounts of slip on the active slip systems remain equal after bifurcation. This usually leads to non-crystallographic shear band orientations (see Table 1), “non-crystallographic” meaning that the orientation of the localization plane depends on both crystallographic directions and the elastic constants. However some slip systems may be deactivated in the band and other modes become possible. In the simple case of symmetric double slip and assuming linear viscosity and hardening, a very simple analysis provides the main trends of the influence of latent hardening on the stability of symmetric multislip localization modes. There exists:

$$\begin{aligned} k\dot{\gamma}_1 &= \tau - \tau_0 - H_{11}\gamma_1 - H_{12}\gamma_2, \\ k\dot{\gamma}_2 &= \tau - \tau_0 - H_{12}\gamma_1 - H_{11}\gamma_2. \end{aligned}$$

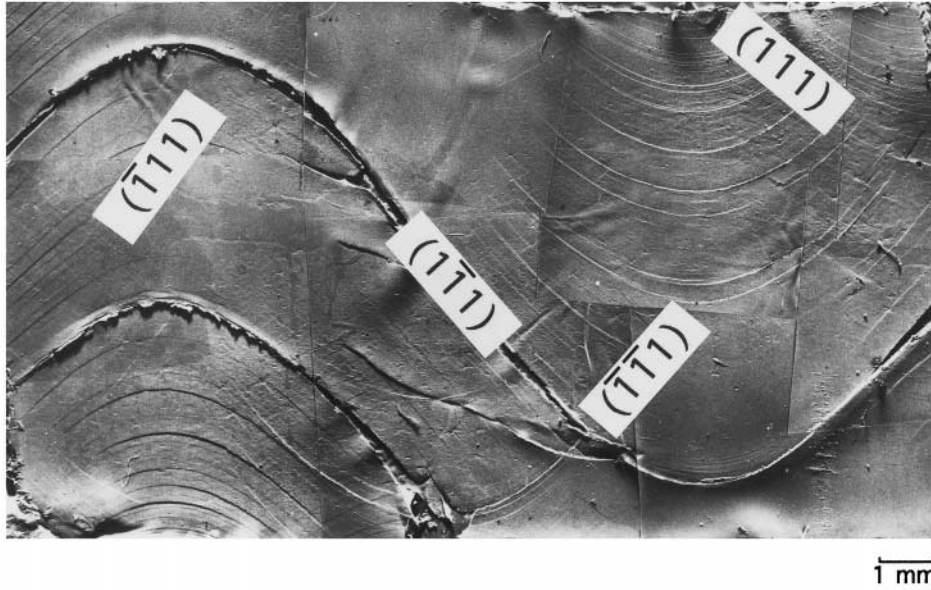


Fig. 3. Tensile test on a (001)-single crystal superalloy AM1, replica of the surface of the cylindrical specimen (after Ref. [14]).

Hence

$$k\Delta\dot{\gamma} = -(H_{11} - H_{12})\Delta\gamma \quad (12)$$

where $\Delta\gamma = \gamma_2 - \gamma_1$. If $H_{11} - H_{12} < 0$, symmetric slip may not be stable, meaning that a small perturbation $\Delta\gamma$ will grow and one slip system may then accommodate the entire plastic deformation.

3.2. Symmetric and symmetry-breaking modes

The formation of slip and shear bands for double slip in tension (single crystal plate: tensile direction [012], secondary direction [521], the systems A3 and B4 are active) has been investigated numerically for various latent hardening ratios. In the following, the hardening law (equation (9)) is used, $H_{11} = q_1 h_{11}$ and $H_{12} = q_1 h_{12}$ are denoted and the material parameters are:

$$\begin{aligned} r_0 &= 50 \text{ MPa}, & q_1 &= -45 \text{ MPa}, \\ b_1 &= 210, & q_2 &= 22 \text{ MPa}, \\ b_2 &= 1800, & k &= 5 \text{ MPa s}^{1/n}, \\ n &= 2 \end{aligned} \quad (13)$$

(global prescribed strain rate $5 \cdot 10^{-5} \text{ s}^{-1}$). The results are the following:

- $h_{11} = 1, h_{12} = 4$: Symmetric slip is stable and the bifurcation modes predicted in Ref. [13] and Table 1 were obtained, with non-crystallographic shear band orientations. Figure 4 shows that the amounts of slip due to the two slip systems in the bands remain equal.

- $h_{11} = 1, h_{12} = 1$ (isotropic hardening): The results are very similar to the previous ones.

- $h_{11} = 2, h_{12} = 1$: In this case, mixed modes are obtained. In one of the two bands the two systems

remain equally active. The other one is a slip band for the system B4 (Fig. 5).

- $h_{11} = 4, h_{12} = 1$: In this case, two slip bands and a kink band are obtained (Fig. 6).

- $h_{11} = 1, h_{12} = 0$ (diagonal matrix): Two slip bands and one kink band formed (Fig. 7).

In Fig. 7, it can be seen that three-dimensional calculations are required to take the actual kinematics of double slip into account, although only one element is used in the thickness. Note that this last result has been obtained using a large strain formulation of crystal plasticity according to classical Mandel's multiplicative decomposition [18]. As expected, slip and kink band can form simultaneously even though lattice rotations are taken into account.

The obtained bifurcation modes are in qualitative agreement with the simple stability analysis of equation (12). It must be noted that softening crystals have been considered so that H_{11} and H_{12} become negative. For softening crystals and strong out of diagonal terms h^{rs} , symmetric slip is stable and non-crystallographic bands may form. When the diagonal components are the biggest ones, slip and kink bands appear because symmetric slip becomes unstable.

4. COSSERAT SINGLE CRYSTAL PLASTICITY

4.1. Shortcomings of classical crystal plasticity

The predictive capabilities of a constitutive model of the plastic behavior of single crystals strongly depends on the accuracy of the description of the dislocation population inside the volume element of mechanics. A complete description of this distri-

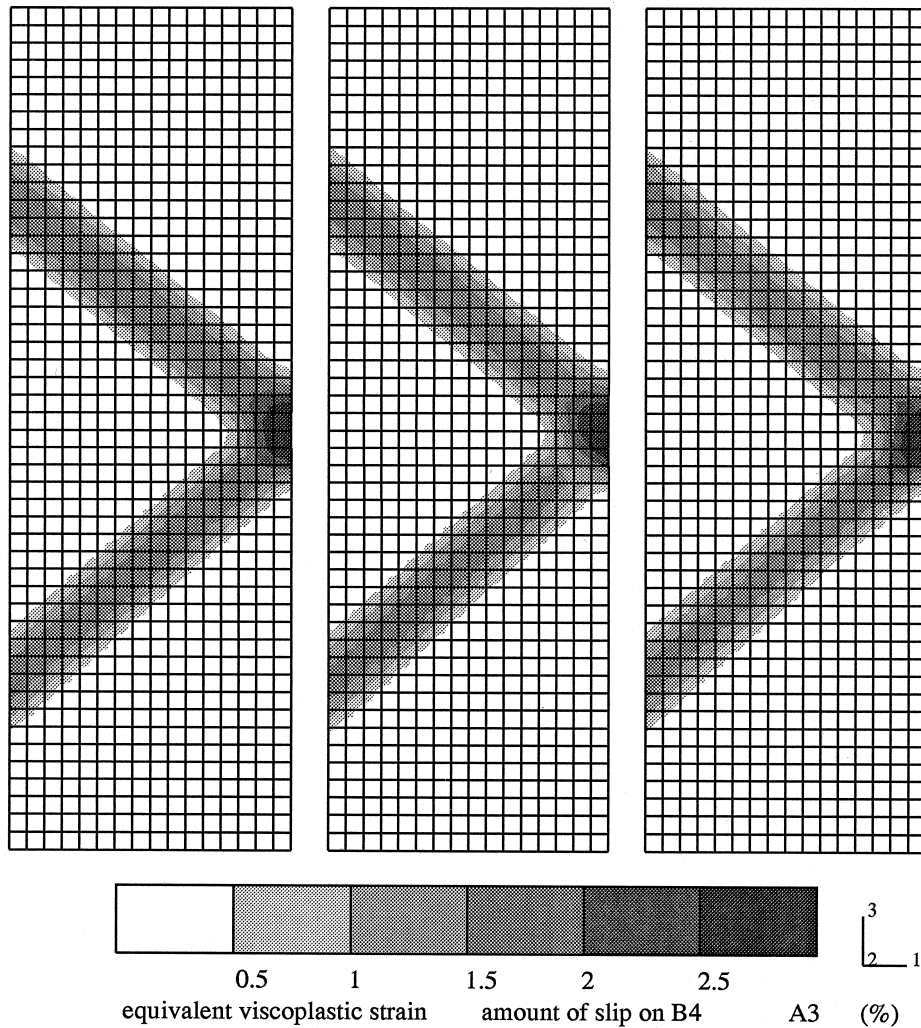


Fig. 4. Shear banding in a single crystal plate oriented for double slip ($h_{11}=1$, $h_{12}=4$); the pictures show the equivalent plastic strain and the amounts of slip for each slip system.

bution would require an infinite set of correlation functions as Kröner pointed out [19]. Only two of them are actually used in practice and in two different contexts.

The continuum theory of dislocations, on the one hand, resorts exclusively to the so-called dislocation density tensor $\tilde{\alpha}$ introduced by Nye [20]. In other terms, $\tilde{\alpha}$ is directly related to the densities of so-called geometrically necessary dislocations [21]. On the other hand, classical crystal plasticity aims at describing the material hardening under homogeneous tension or shear for instance, where $\tilde{\alpha}$ does not play an important role. As a result, classical crystal plasticity theory involves a set of internal variables which are related to the scalar dislocations densities ρ^s traditionally used in metallurgy. The ρ^s denote in fact the densities of so-called statistically stored dislocations [21]. However, in the case of strongly non-homogeneous deformation, $\tilde{\alpha}$ may well be predominant.

A more accurate theory should combine both descriptions. This can be done within the framework of a non local continuum and in particular of a Cosserat theory as explained in Ref. [22].

Another rather puzzling aspect of classical crystal plasticity that arises from the previous localization analyses is that it predicts that slip and kink bands can appear simultaneously for the same critical hardening modulus. But slip and kink bands are very different localization modes from the physical point of view. As illustrated on Fig. 8, kink banding is associated with strong lattice rotation whereas slip banding does not affect crystal orientation (except in the case of some boundary constraints). The three-dimensional analysis is performed in order to see whether additional slip systems are activated. For the considered amount of lattice rotation inside the band, additional slip systems are not significantly activated. Accordingly, a kink band is bounded by two thin regions of intense lat-

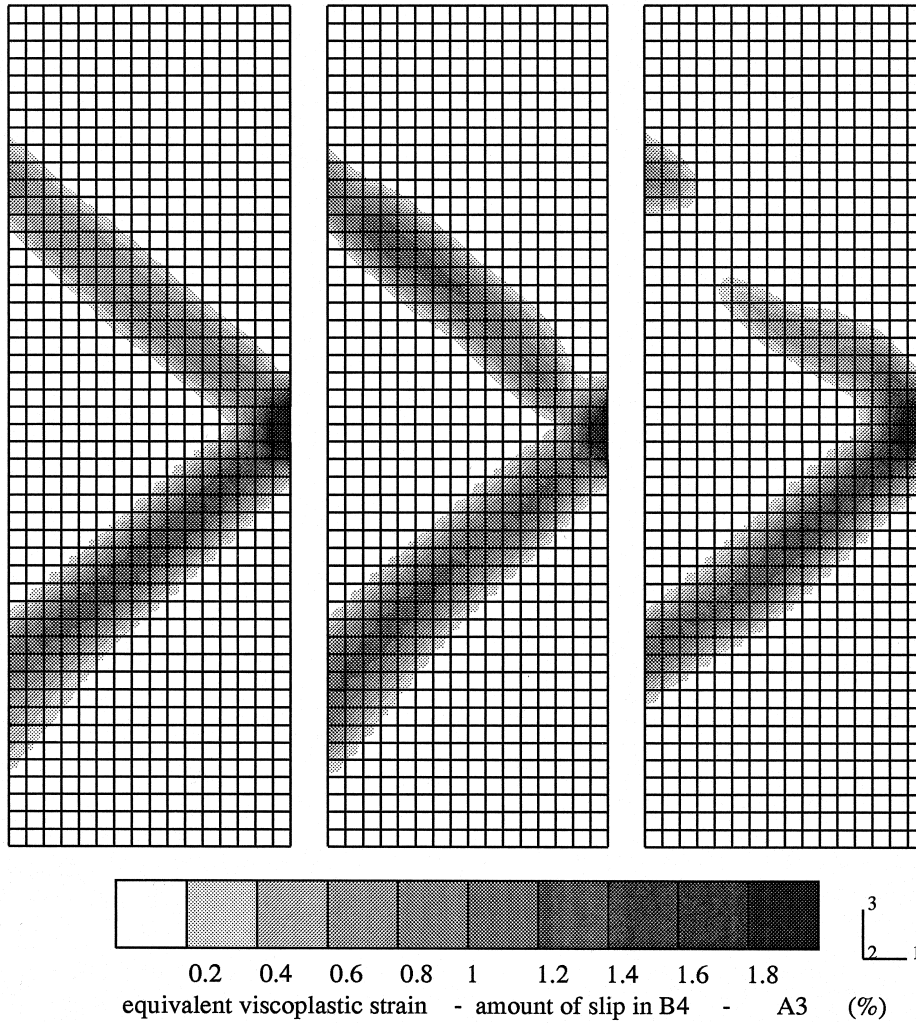


Fig. 5. Shear and slip band formation in a single crystal plate oriented for double slip ($h_{11}=2, h_{12}=1$).

tice curvature associated with high densities of geometrically necessary dislocations. Furthermore, kink bands are in general not observed at incipient plasticity in f.c.c. crystals but, if at all, much later on (see Section 1). The fact that classical crystal plasticity does not really distinguish the onsets of slip and kink banding should be regarded as a shortcoming. This also motivates the following developments.

4.2. Model presentation

The proposed Cosserat theory for elastoviscoplastic single crystals has been comprehensively presented in Ref. [22] with full account of finite deformation and curvature. The equations of the model in the case of small perturbations are simply recalled, which means small displacement, lattice rotation, deformation and lattice curvature.

The displacement vector at point \bar{x} is denoted by $\bar{u}(\bar{x})$. The lattice rotation $\tilde{\mathbf{R}}(\bar{x})$ with respect to its initial orientation is described by vector $\bar{\Phi}(\bar{x})$ such that:

$$\tilde{\mathbf{R}} = \tilde{\mathbf{I}} - \bar{\epsilon}\bar{\Phi}, R_{ij} = \delta_{ij} - \epsilon_{ijk}\Phi_k \quad (14)$$

where ϵ is the permutation tensor. The Cosserat deformation tensor is

$$\tilde{\epsilon} = \bar{u} \otimes \bar{\nabla} + \bar{\epsilon}\bar{\Phi}, e_{ij} = u_{i,j} + \epsilon_{ijk}\Phi_k \quad (15)$$

and the lattice torsion-curvature tensor reads:

$$\tilde{\kappa} = \bar{\Phi} \otimes \bar{\nabla}, \kappa_{ij} = \Phi_{i,j}. \quad (16)$$

Both deformation and curvature tensors must be decomposed into their elastic and plastic parts:

$$\tilde{\epsilon} = \tilde{\epsilon}^e + \tilde{\epsilon}^p, \quad \tilde{\kappa} = \tilde{\kappa}^e + \tilde{\kappa}^p. \quad (17)$$

The elasticity law in the isotropic case reads:

$$\tilde{\sigma} = \mathbf{E}:\tilde{\epsilon}^e = \lambda \tilde{\mathbf{I}} \text{Tr} \tilde{\epsilon}^e + 2\mu\{\tilde{\epsilon}^e\} + 2\mu_c\tilde{\epsilon}^e \quad (18)$$

$$\tilde{\mu} = \mathbf{C}:\tilde{\kappa}^e = \alpha \tilde{\mathbf{I}} \text{Tr} \tilde{\kappa}^e + 2\beta\{\tilde{\kappa}^e\} + 2\gamma\tilde{\kappa}^e \quad (19)$$

where $\tilde{\sigma}$ and $\tilde{\mu}$, respectively, are the force and couple stress tensors. The inverted brackets denote

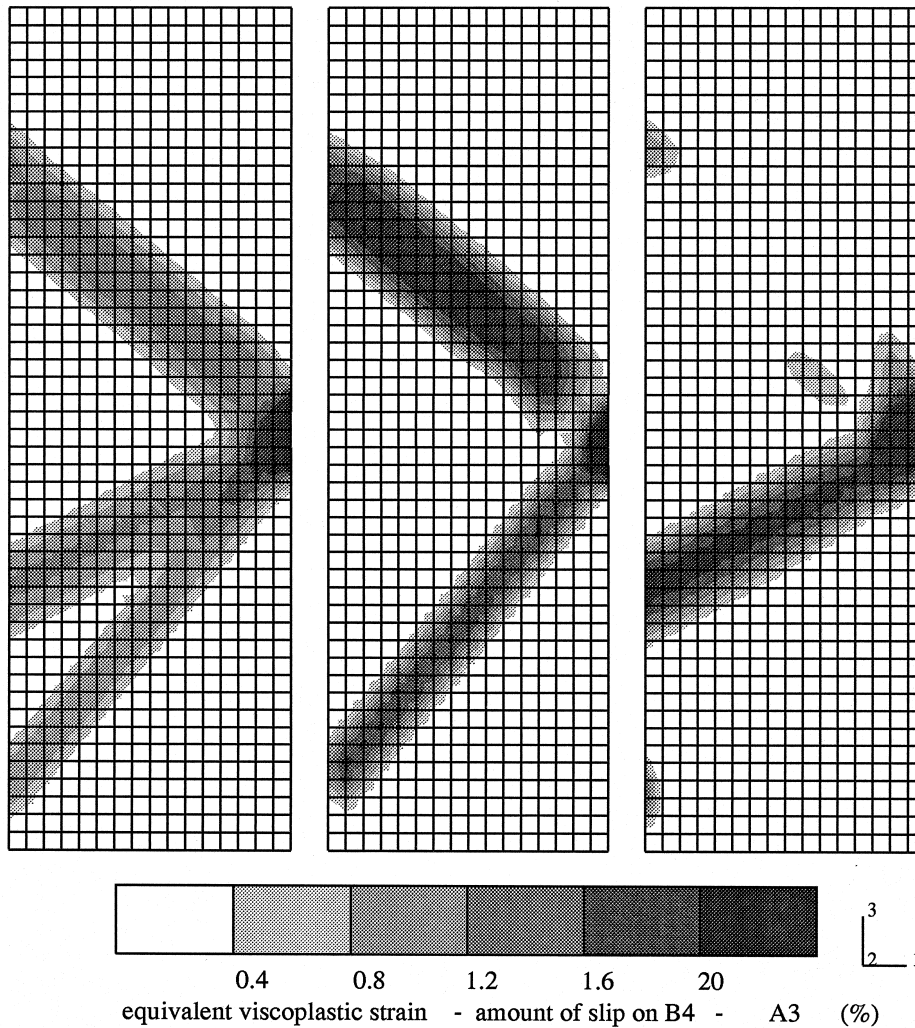


Fig. 6. Slip and kink band formation in a single crystal plate oriented for double slip ($h_{11}=4, h_{12}=1$).

the skew-symmetric part. Equations (18) and (19) involve 6 elasticity moduli, the 2 classical ones and four additional ones.

Plastic deformation is due to the activation of slip systems according to

$$\dot{\epsilon}^p = \sum_{s=1}^n \dot{\gamma}^s \tilde{\mathbf{P}}^s \quad (20)$$

Similarly, plastic torsion-curvature orientation tensors $\tilde{\mathbf{Q}}_{\perp}$ and $\tilde{\mathbf{Q}}_{\odot}$ exist such that

$$\dot{\kappa}^p = \sum_{s=1}^n \left(\frac{\dot{\theta}_{\perp}^s}{l_{\perp}} \tilde{\mathbf{Q}}_{\perp}^s + \frac{\dot{\theta}_{\odot}^s}{l_{\odot}} \tilde{\mathbf{Q}}_{\odot}^s \right) \quad (21)$$

where l_{\perp}, l_{\odot} are constitutive characteristic lengths. The index \perp denotes lattice curvature due to edge dislocations and \odot accounts for lattice torsion due to screw dislocations. The continuum theory of dislocations provides a relationship between the dislocation density tensor and the torsion-curvature tensor [22, 23], from which is deduced

$$\tilde{\mathbf{Q}}_{\perp} = \bar{\xi} \otimes \bar{\mathbf{m}}, \quad \tilde{\mathbf{Q}}_{\odot} = \frac{1}{2} \tilde{\mathbf{I}} - \bar{\mathbf{m}} \otimes \bar{\mathbf{m}} \quad (22)$$

where $\bar{\xi} = \bar{\mathbf{z}} \times \bar{\mathbf{m}}$ is the edge dislocation line vector.

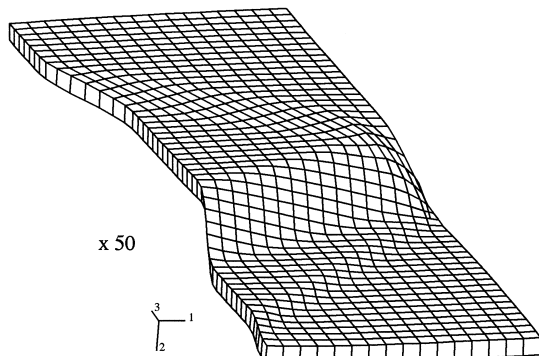


Fig. 7. Slip and kink band formation in a single crystal plate oriented for double slip ($h_{11}=1, h_{12}=0$); three-dimensional deformed state.

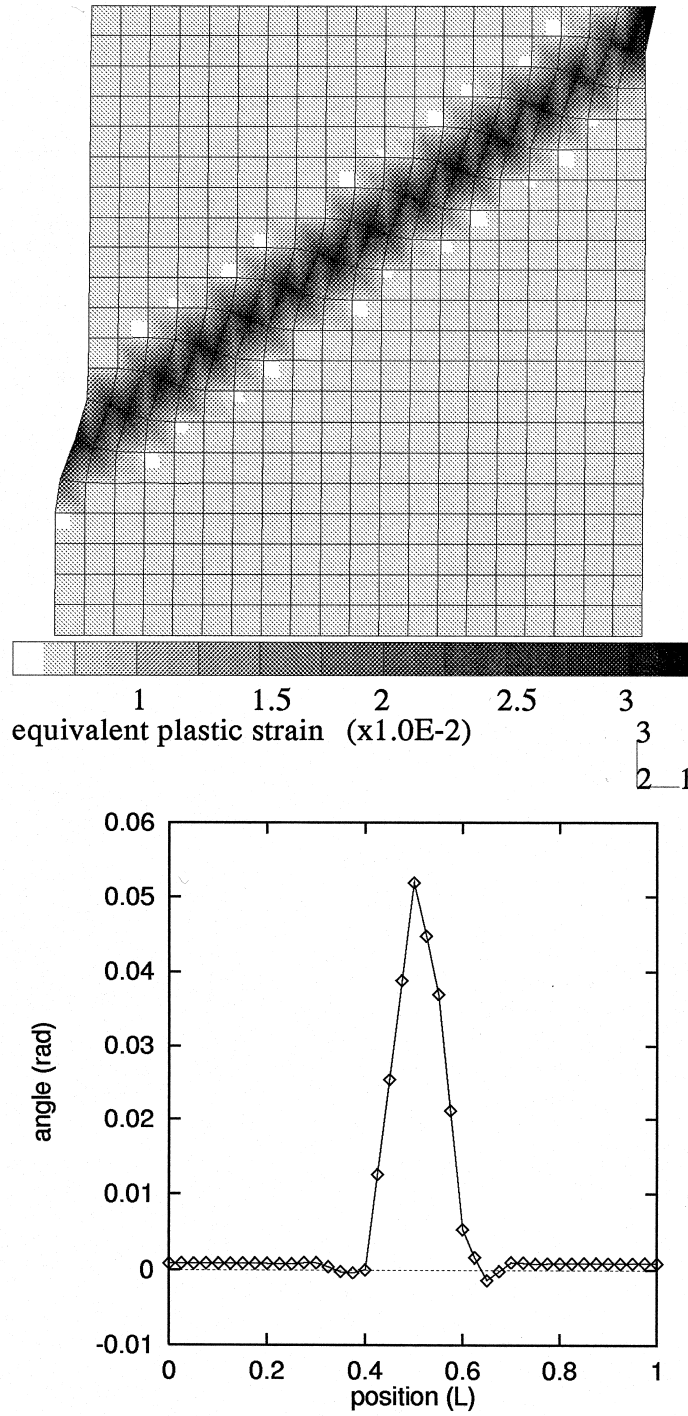


Fig. 8. Kink band formation in a single crystal: amount of plastic strain (above) and associated lattice rotation along a horizontal line intersecting the band (below).

The viscoplastic formulation (equation (11)) for the plastic slip rate is still adopted, where $\tau^s = \tilde{\sigma} : \tilde{\mathbf{P}}^s$. Note that the force–stress tensor $\tilde{\sigma}$ is not necessarily symmetric. Similarly and for reasons presented in Ref. [22], a generalized Schmid law and a curvature flow rule are introduced:

$$\dot{\theta}^s = \left\langle \frac{|v^s| - lr_c^s}{lk_c^s} \right\rangle^{n_c} \text{sign}(v^s) \quad (23)$$

with $v^s = \tilde{\boldsymbol{\mu}} : \tilde{\mathbf{Q}}^s$. General hardening laws are proposed in Ref. [22] and particular ones will be used in the sequel.

5. BIFURCATION ANALYSIS FOR COSSERAT CRYSTALS

In the case of single slip a bifurcation analysis in Cosserat elastoplasticity is now performed in order to see the new features brought by the Cosserat theory.

5.1. A simple case

We first consider the case of single slip $\tilde{\mathbf{P}} = \tilde{\mathbf{m}} \otimes \tilde{\mathbf{z}}$ before plastic curvature appears and it is asked whether the slip bands and kink bands studied in Section 2 are still bifurcation modes for Cosserat crystals or not (see equations (1) and (2)).

5.1.1. *Slip band: $\tilde{\mathbf{g}} \propto \tilde{\mathbf{m}}$ (glide direction) $\tilde{\mathbf{n}} = \tilde{\mathbf{z}}$ (slip plane).* We investigate the existence of a discontinuity surface of normal $\tilde{\mathbf{n}} = \tilde{\mathbf{z}}$ with the jump

$$\llbracket \tilde{\mathbf{e}} \rrbracket \propto \tilde{\mathbf{m}} \otimes \tilde{\mathbf{z}} \quad (24)$$

The equilibrium condition at the interface reads

$$\llbracket \tilde{\boldsymbol{\sigma}} \rrbracket \tilde{\mathbf{z}} = 0 \quad (25)$$

Assuming plastic loading on each side, it follows

$$\llbracket \mathbf{L} \tilde{\mathbf{e}} \rrbracket \tilde{\mathbf{z}} = 0, \quad \text{i.e. } (\mathbf{L} \tilde{\mathbf{P}}) \tilde{\mathbf{z}} = 0 \quad (26)$$

where the tangent moduli are defined in equation (35). Taking $i^s = H\dot{\gamma}$, it gives

$$E_{ijkl} P_{kl} z_j - \frac{1}{H + P_{ab} E_{abcd} P_{cd}} E_{ijkl} P_{kl} P_{nm} E_{mnpq} P_{pq} z_j = 0. \quad (27)$$

It can be checked immediately that $H = 0$ is still a solution of equation (27). It means that under the above hypotheses, slip bands are still possible and lead to the loss of ellipticity of the equations as soon as the hardening modulus vanishes.

5.1.2. *Kink band: $\tilde{\mathbf{g}} \propto \tilde{\mathbf{z}}$, $\tilde{\mathbf{n}} = \tilde{\mathbf{m}}$.* We must have now

$$(\mathbf{L} \tilde{\mathbf{P}}^T) \tilde{\mathbf{m}} = 0. \quad (28)$$

This implies

$$\tilde{\mathbf{z}} \cdot (\mathbf{L} \tilde{\mathbf{P}}^T) \cdot \tilde{\mathbf{m}} = 0$$

and hence

$$\tilde{\mathbf{P}}^T : \mathbf{E} : \tilde{\mathbf{P}}^T - \frac{(\tilde{\mathbf{P}}^T : \mathbf{E} : \tilde{\mathbf{P}})(\tilde{\mathbf{P}} : \mathbf{E} : \tilde{\mathbf{P}}^T)}{H + \tilde{\mathbf{P}} : \mathbf{E} : \tilde{\mathbf{P}}} = 0. \quad (29)$$

One obtains the critical hardening modulus for which a kink band may appear

$$H^{\text{kink}} = \frac{(\tilde{\mathbf{P}}^T : \mathbf{E} : \tilde{\mathbf{P}})^2}{\tilde{\mathbf{P}}^T : \mathbf{E} : \tilde{\mathbf{P}}} - \tilde{\mathbf{P}} : \mathbf{E} : \tilde{\mathbf{P}}. \quad (30)$$

For isotropic elasticity

$$H^{\text{kink}} = -\frac{4\mu\mu_c}{\mu + \mu_c} < 0. \quad (31)$$

Equation (28) is then fulfilled.

As a result the loss of ellipticity for the kink band is delayed. The elastic Cosserat modulus, μ_c is

responsible for this regularizing effect. For $\mu_c = 0$ the classical result is retrieved.

5.2. General case

Both plastic deformation and curvature are now considered:

$$\dot{\tilde{\mathbf{e}}}^p = \dot{\gamma} \tilde{\mathbf{P}} \quad \text{and} \quad \dot{\tilde{\boldsymbol{\kappa}}}^p = \frac{\dot{\theta}}{l} \tilde{\mathbf{Q}} \quad (32)$$

where $\tilde{\mathbf{P}} = \tilde{\mathbf{m}} \otimes \tilde{\mathbf{z}}$ and $\tilde{\mathbf{Q}} = \tilde{\boldsymbol{\zeta}} \otimes \tilde{\mathbf{m}}$ meaning that edge dislocations only are considered. The retained hardening rules are

$$i^s = \tilde{\mathbf{P}} : \dot{\tilde{\boldsymbol{\sigma}}} = H\dot{\gamma} + H'\dot{\theta} \quad (33)$$

$$i_c^s = \frac{1}{l} \tilde{\mathbf{Q}} : \dot{\tilde{\boldsymbol{\mu}}} = H_c \dot{\theta} \quad (34)$$

where the instantaneous curvature hardening modulus H_c and the coupling term H' have been introduced. Note that a thermodynamically consistent formulation of the model like in Ref. [22] leads to a symmetric coupling term in equation (34), which is not included in the present analysis for simplicity. The linear incremental form of the constitutive equations can be derived

$$\dot{\tilde{\boldsymbol{\sigma}}} = \mathbf{L} : \dot{\tilde{\mathbf{e}}} + \mathbf{L}' : \dot{\tilde{\boldsymbol{\kappa}}} \quad \dot{\tilde{\boldsymbol{\mu}}} = \mathbf{L}^c : \dot{\tilde{\boldsymbol{\kappa}}} \quad (35)$$

with

$$\mathbf{L} = \mathbf{E} - \frac{1}{\Delta} (\mathbf{E} : \tilde{\mathbf{P}}) \otimes (\tilde{\mathbf{P}} : \mathbf{E}) \quad (36)$$

$$\mathbf{L}' = \frac{H'}{l\Delta\Delta_c} (\mathbf{E} : \tilde{\mathbf{P}}) \otimes (\tilde{\mathbf{Q}} : \mathbf{C}) \quad (37)$$

$$\mathbf{L}^c = \mathbf{C} - \frac{1}{l^2\Delta_c} (\mathbf{C} : \tilde{\mathbf{Q}}) \otimes (\tilde{\mathbf{Q}} : \mathbf{C}) \quad (38)$$

and

$$\Delta = H + \tilde{\mathbf{P}} : \mathbf{E} : \tilde{\mathbf{P}} \quad (39)$$

$$\Delta^c = H^c + \tilde{\mathbf{Q}} : \mathbf{C} : \tilde{\mathbf{Q}} / l^2 \quad (40)$$

We investigate the conditions for the existence of a surface S across which $\tilde{\mathbf{e}}$ and $\tilde{\boldsymbol{\kappa}}$ are discontinuous. Let $\tilde{\mathbf{n}}$ be the normal to the surface at $\tilde{\mathbf{x}} \in S$. Hadamard compatibility conditions imply that the jumps are of the form

$$\exists(\tilde{\mathbf{g}}, \tilde{\mathbf{g}}^c) / \llbracket \tilde{\mathbf{e}} \rrbracket = \tilde{\mathbf{g}} \otimes \tilde{\mathbf{n}} \quad \text{and} \quad \llbracket \tilde{\boldsymbol{\kappa}} \rrbracket = \tilde{\mathbf{g}}^c \otimes \tilde{\mathbf{n}}. \quad (41)$$

The equilibrium conditions are given by

$$\llbracket \tilde{\boldsymbol{\sigma}} \rrbracket \tilde{\mathbf{n}} = 0 \quad \text{and} \quad \llbracket \tilde{\boldsymbol{\mu}} \rrbracket \tilde{\mathbf{n}} = 0. \quad (42)$$

They lead to the following conditions

$$\left(\tilde{\mathbf{n}} \cdot \mathbf{E} \cdot \tilde{\mathbf{n}} - \frac{1}{\Delta} (\tilde{\mathbf{n}} : \mathbf{E} : \tilde{\mathbf{P}}) \otimes (\tilde{\mathbf{P}} : \mathbf{E} : \tilde{\mathbf{n}}) \right) \tilde{\mathbf{g}} + \frac{H'}{l\Delta\Delta_c} ((\tilde{\mathbf{n}} : \mathbf{E} : \tilde{\mathbf{P}}) \otimes (\tilde{\mathbf{Q}} : \mathbf{C} : \tilde{\mathbf{n}})) \tilde{\mathbf{g}}^c = 0 \quad (43)$$

$$\left(\bar{\mathbf{n}} \cdot \mathbf{C} \cdot \bar{\mathbf{n}} - \frac{1}{l^2 \Delta_c} (\bar{\mathbf{n}} \cdot \mathbf{C} : \tilde{\mathbf{Q}}) \otimes (\tilde{\mathbf{Q}} : \mathbf{C} \cdot \bar{\mathbf{n}}) \right) \bar{\mathbf{g}}^c = 0. \quad (44)$$

Note that short notations have been adopted but it must be noticed that by $\bar{\mathbf{n}} \cdot \mathbf{E} \cdot \bar{\mathbf{n}}$, $n_j E_{ijk} n_l$ is meant here. This holds also for some other expressions that are not explicitly written in components.

Following [15], the solution of equation (44) is

$$\bar{\mathbf{g}}^c \propto (\bar{\mathbf{n}} \cdot \mathbf{C} \cdot \bar{\mathbf{n}})^{-1} (\bar{\mathbf{n}} \cdot \mathbf{C} : \tilde{\mathbf{Q}}) / l \quad (45)$$

$$l^2 H^c = -\tilde{\mathbf{Q}} : \mathbf{C} : \tilde{\mathbf{Q}} + (\tilde{\mathbf{Q}} : \mathbf{C} \cdot \bar{\mathbf{n}}) (\bar{\mathbf{n}} \cdot \mathbf{C} \cdot \bar{\mathbf{n}})^{-1} (\bar{\mathbf{n}} \cdot \mathbf{C} : \tilde{\mathbf{Q}}). \quad (46)$$

Restriction to isotropic elasticity now occurs and for that purpose, the tensors \mathbf{I} , \mathbf{I}^a and \mathbf{J} , \mathbf{J}^a , \mathbf{K} are introduced, such that

$$\mathbf{I}\tilde{\mathbf{e}} = \{\tilde{\mathbf{e}}\} \quad \text{and} \quad \mathbf{I}^a \tilde{\mathbf{e}} = \mathbf{J}\tilde{\mathbf{e}} = \mathbf{J}^a \tilde{\mathbf{e}} = \{\tilde{\mathbf{e}}\} \quad (47)$$

$$\mathbf{K}\tilde{\mathbf{e}} = \frac{\text{tr } \tilde{\mathbf{e}}}{3} \tilde{\mathbf{I}} \quad \text{and} \quad \mathbf{J}\tilde{\mathbf{e}} = \{\tilde{\mathbf{e}}\} - \frac{\text{tr } \tilde{\mathbf{e}}}{3} \tilde{\mathbf{I}} \quad (48)$$

and

$$\mathbf{K} + \mathbf{J} + \mathbf{J}^a = \mathbf{I} + \mathbf{I}^a = \mathbf{1} \quad (49)$$

where $\mathbf{1}$ is the identity linear operator on non-symmetric second-rank tensors. As a result the isotropic elasticity tensors can be written

$$\mathbf{C} = 3\alpha \mathbf{K} + 2\beta \mathbf{I} + 2\gamma \mathbf{I}^a = (3\alpha + 2\beta) \mathbf{K} + 2\beta \mathbf{J} + 2\gamma \mathbf{J}^a. \quad (50)$$

Similar relationships hold for \mathbf{E} . There exists a very convenient property

$$\mathbf{C}^{-1} = \frac{1}{3\alpha + 2\beta} \mathbf{K} + \frac{1}{2\beta} \mathbf{J} + \frac{1}{2\gamma} \mathbf{J}^a. \quad (51)$$

As a result

$$\bar{\mathbf{n}} \cdot \mathbf{C} \cdot \bar{\mathbf{n}} = (\beta + \gamma) \tilde{\mathbf{I}} + (\alpha + \beta - \gamma) \bar{\mathbf{n}} \otimes \bar{\mathbf{n}} \quad (52)$$

and

$$(\bar{\mathbf{n}} \cdot \mathbf{C} \cdot \bar{\mathbf{n}})^{-1} = \frac{1}{\beta + \gamma} \tilde{\mathbf{I}} - \frac{\alpha + \beta - \gamma}{(\beta + \gamma)(\alpha + 2\beta)} \bar{\mathbf{n}} \otimes \bar{\mathbf{n}} \quad (53)$$

We get from equation (45)

$$\begin{aligned} \bar{\mathbf{g}}^c = g^c & \left((\bar{\mathbf{n}} \cdot \bar{\mathbf{m}}) \bar{\xi} + \frac{\beta - \gamma}{\beta + \gamma} (\bar{\mathbf{n}} \cdot \bar{\xi}) \bar{\mathbf{m}} \right. \\ & \left. - \frac{2\gamma(\alpha + \beta - \gamma)}{(\beta + \gamma)(\alpha + 2\beta)} (\bar{\mathbf{n}} \cdot \bar{\mathbf{m}}) (\bar{\mathbf{n}} \cdot \bar{\xi}) \bar{\mathbf{n}} \right) \end{aligned} \quad (54)$$

and from equation (46)

$$\begin{aligned} l^2 H^c = (\beta + \gamma) & ((\bar{\mathbf{n}} \cdot \bar{\mathbf{m}})^2 - 1) + \frac{(\beta - \gamma)^2}{\beta + \gamma} (\bar{\mathbf{n}} \cdot \bar{\xi})^2 \\ & - (\bar{\mathbf{n}} \cdot \bar{\mathbf{m}})^2 (\bar{\mathbf{n}} \cdot \bar{\xi})^2 \frac{4\beta\gamma(\alpha + \beta - \gamma)}{(\alpha + 2\beta)(\beta + \gamma)}. \end{aligned} \quad (55)$$

Equations (54) and (55) must now be substituted in equation (43). At this stage, coordinates relative to

the basis $(\bar{\mathbf{m}}, \bar{\mathbf{z}}, -\bar{\xi})$ are resorted to. This leads to the following system of equations

$$\begin{aligned} & (\mu + \mu_c) \begin{bmatrix} g_1 \\ g_2 \\ g_3 \end{bmatrix} + (\lambda + \mu - \mu_c) (n_i g_i) \begin{bmatrix} n_1 \\ n_2 \\ n_3 \end{bmatrix} \\ & - \frac{1}{\Delta} ((\mu + \mu_c) n_2 g_1 + (\mu - \mu_c) n_1 g_2) \\ & \times \left((\mu + \mu_c) n_2 \begin{bmatrix} 1 \\ 0 \\ 0 \end{bmatrix} + (\mu - \mu_c) n_1 \begin{bmatrix} 0 \\ 1 \\ 0 \end{bmatrix} \right) \\ & + \frac{H' g^c}{l \Delta \Delta^c} \left((\beta + \gamma) n_1^2 + \frac{(\beta - \gamma)^2}{\beta + \gamma} n_3^2 \right. \\ & \left. - \frac{4\beta\gamma(\alpha + \beta - \gamma)}{(\alpha + 2\beta)(\beta + \gamma)} n_1^2 n_3^2 \right) \\ & \times \left((\mu + \mu_c) n_2 \begin{bmatrix} 1 \\ 0 \\ 0 \end{bmatrix} + (\mu - \mu_c) n_1 \begin{bmatrix} 0 \\ 1 \\ 0 \end{bmatrix} \right) = 0 \end{aligned}$$

Two cases can be distinguished but the details of the calculation are not given:

• $n_3 = 0$:

Then $g_3 = 0$ and

$$\begin{aligned} g_1 = - \frac{H' g^c}{\Delta \Delta^c} & (\beta + \gamma) n_1^2 n_2 \left((\mu + \mu^c) ((\mu + \mu_c) \right. \\ & \left. + (\lambda + \mu - \mu_c) n_2^2 - \frac{1}{\Delta} (\mu - \mu_c)^2 n_1^2) \right. \\ & \left. - (\mu - \mu_c) n_1^2 ((\lambda + \mu - \mu_c) - \frac{1}{\Delta} (\mu^2 - \mu_c^2)) \right) / D \end{aligned} \quad (56)$$

$$\begin{aligned} g_2 = - \frac{H' g^c}{\Delta \Delta^c} & (\beta + \gamma) n_1^3 \left((\mu - \mu^c) ((\mu + \mu_c) \right. \\ & \left. + (\lambda + \mu - \mu_c) n_2^2 - \frac{1}{\Delta} (\mu + \mu_c)^2 n_1^2) \right. \\ & \left. - (\mu + \mu_c) n_2^2 ((\lambda + \mu - \mu_c) - \frac{1}{\Delta} (\mu^2 - \mu_c^2)) \right) / D \end{aligned} \quad (57)$$

where D is the determinant of the system.

• $n_3 \neq 0$: For the sake of simplicity, the expressions are not given in this case.

5.2.1. *Extrema of $H^c(\bar{\mathbf{n}})$* . We now look for the critical hardening modulus for which the first plastic/plastic bifurcation becomes possible. As in Ref. [13], the Lagrangian function is considered

$$L(\bar{\mathbf{n}}, \lambda) = H^c(\bar{\mathbf{n}}) - \lambda (n_1^2 + n_2^2 + n_3^2 - 1). \quad (58)$$

When written in components, equation (46) becomes

$$H_c(\bar{\mathbf{n}}) = (\beta + \gamma)(n_1^2 - 1) + \frac{(\beta - \gamma)^2}{\beta + \gamma} n_3^2 - n_1^2 n_3^2 \frac{4\beta\gamma(\alpha + \beta - \gamma)}{(\alpha + 2\beta)(\beta + \gamma)} \quad (59)$$

The maximization procedure leads to the three following cases:

- $\bar{\mathbf{n}} = \bar{\xi}$: However, this implies $\bar{\mathbf{g}}^c = \bar{\mathbf{g}} = 0$. No bifurcation is possible in that case.

- $\bar{\mathbf{n}} = \bar{\mathbf{m}}$ and $\mathbf{g}^c \bar{\xi}$:

Then

$$\bar{\mathbf{g}} = -g^c \frac{H'(\mu - \mu_c)}{l(H(\mu + \mu_c) + 4\mu\mu_c)} \bar{\mathbf{z}}. \quad (60)$$

This corresponds to a kink band. Contrary to the classical case, for a given amplitude of the curvature rate jump g^c at the surface, the amplitude of the strain rate jump is no longer arbitrary. The critical hardening modulus is

$$H_c = 0. \quad (61)$$

The case $g^c = 0$ has already been treated in Section 5.1.

- $n_1 n_3 \neq 0$:

In this case, $H^c < 0$ is found.

5.2.2. *Conclusion of the bifurcation analysis.* If curvature and deformation are decoupled (no lattice rotation gradients), slip bands are still possible bifurcation modes (Section 5.1). In the coupled case, the first possible mode is the kink band that can appear if the Cosserat hardening modulus H^c vanishes. The use of a positive H^c leads to the regularization of the kink band. If a coupling exists between slip and curvature in equation (34) the amplitudes of the deformation rate and curvature rate jumps are not arbitrary any more.

5.3. Simulation of localization modes in Cosserat crystals

It is possible to perform three-dimensional FE calculations using the previous model, although it involves many degrees of freedom and internal variables. At each node, the six degrees of freedom are the displacement $\bar{\mathbf{u}}$ and the lattice rotation $\bar{\Phi}$. At each Gauss point, 36 internal variables must be integrated, namely the v^s , θ_\perp^s and θ_\circ^s . For simplicity the θ_\circ^s is not introduced.

To illustrate a major difference between the Cosserat theory and classical plasticity, the tension of a plate (of size $1L$ unit length) oriented for single slip with a material defect leading to kink band formation in the classical case [Fig. 8(a), axis 3][[238], axis 1][[19101]] is considered again.

Let us firstly investigate the influence of Cosserat elasticity on kink banding. The chosen additional elastic constants are, $\mu_c = 100000$ MPa, $\beta = \gamma = 1000$ MPa L^2 , $\alpha = 0$. The hardening law reads

$$r = r_0 + q_1(1 - \exp(-b_1 v)) + q_2(1 - \exp(-b_2 v)) + H' \theta \quad (62)$$

(single slip) with the same material parameters as in (10) and additionally: $H' = 600$ MPa. A high value of r_0^c is chosen so that curvature remains purely elastic. The applied boundary conditions are the following: prescribed displacements of the lower and upper sides of the plate in direction 3, the whole boundary is free of forces (except on the upper and lower sides in direction 3) and micro-couples. On Fig. 11 the overall load–displacement curve of this test is compared to the homogeneous response (strain-softening material) and to the classical response characterized by a sharp load drop corresponding to kink band formation. Instead the curve follows the homogeneous one until a deviation is observed corresponding to the formation of two slip bands (Fig. 9), although the position of the defect would rather promote kink banding. Additional slip systems are not significantly activated.

Plastic curvature is now introduced, which seems to be physically more relevant. The Cosserat elasticity constants are now taken so small that the classical elastic response of the material is unaffected. The additional parameters are:

$$\begin{aligned} r_c^0 &= 0.0005 \text{ MPa}, & k_c &= 0.01 \text{ MPa s}^{1/n_c}, \\ n_c &= 1, & l &= 1L, & H_c &= 0. \end{aligned} \quad (63)$$

In this case again, the expected kink band does not form. Instead, a slip band forms [Fig. 10(a)] and a reflected kink band tends to form. Finally this deformation pattern is replaced by a slip band bundle [Fig. 10(b)]. Figure 11 shows the load drop associated with localization and subsequent hardening due to the local site of plastic curvature at the intersection of the band and the boundary with prescribed displacements.

In the two cases, kink band formation has been precluded leading to preferred slip band formation.

6. CONCLUSIONS

We have shown that classical crystal plasticity can account for several observed localization phenomena like slip, kink and shear band formation in single crystals. Depending on the *latent/self* hardening ratio, symmetric multislip configurations may be stable or not. Since non-crystallographic shear bands like in Fig. 4 are usually not observed experimentally at the inception of plastic flow, the present results would advocate for leading diagonal terms in the interaction matrix, at least in the softening regime of the material behavior.

There exist several generalized crystal plasticity models in literature that usually involve higher order gradients. Second order gradients of the amount of slip or dislocation densities can be intro-

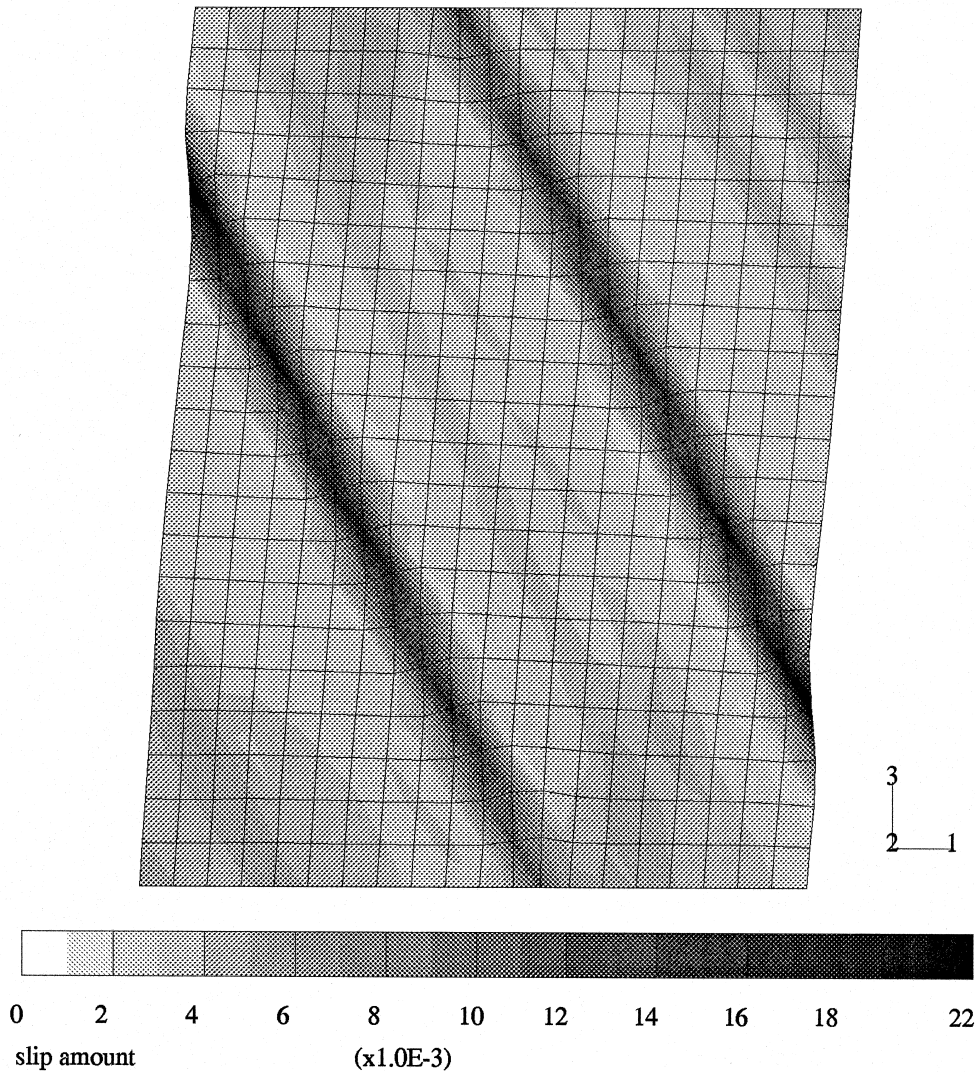


Fig. 9. Slip band formation in a Cosserat crystal supporting only elastic curvature: kink band formation like in Fig. 8 has been precluded.

duced in the hardening law of each slip system as proposed in Ref. [24]. The theory used in Ref. [25] is a full second gradient theory within the framework set in Refs [27,28]. The resulting kinematics of plastic lattice torsion-curvature proposed in Ref. [26] is the same as that derived in the work from the continuum theory of dislocations, so that the second gradient and the Cosserat theory of crystal plasticity share several common features. However the link between the dislocated crystal and the Cosserat continuum has been seen since Günther [29] and Kröner [30]. Furthermore the Cosserat theory presented in Ref. [22] is a natural extension of Mandel's work in finite crystal plasticity [18].

The aim of such a generalized crystal plasticity theory is not the regularization of localization modes in crystals but the enrichment of the continuum description of dislocation population. The

main result of the bifurcation analysis presented in Section 5 is that the bifurcation modes slip/kink bands which are identically predicted by the classical theory, have been separated: kink bands can occur later than skip bands, as observed experimentally. The new critical hardening modulus for kink banding has been given. The FE simulations have shown that kink bands may even be precluded. However, the Cosserat theory does not affect slip banding at all since slip banding induces no lattice curvature. This statement also holds in the case of second grade crystal plasticity [25] since, as pointed out in Ref. [26], a slip gradient along the normal to the slip plane does not result in the storage of geometrically necessary dislocations. It means that the Cosserat and second grade theories do not regularize slip banding in the static case.

The biggest remaining issue is the determination of the additional parameters arising in generalized

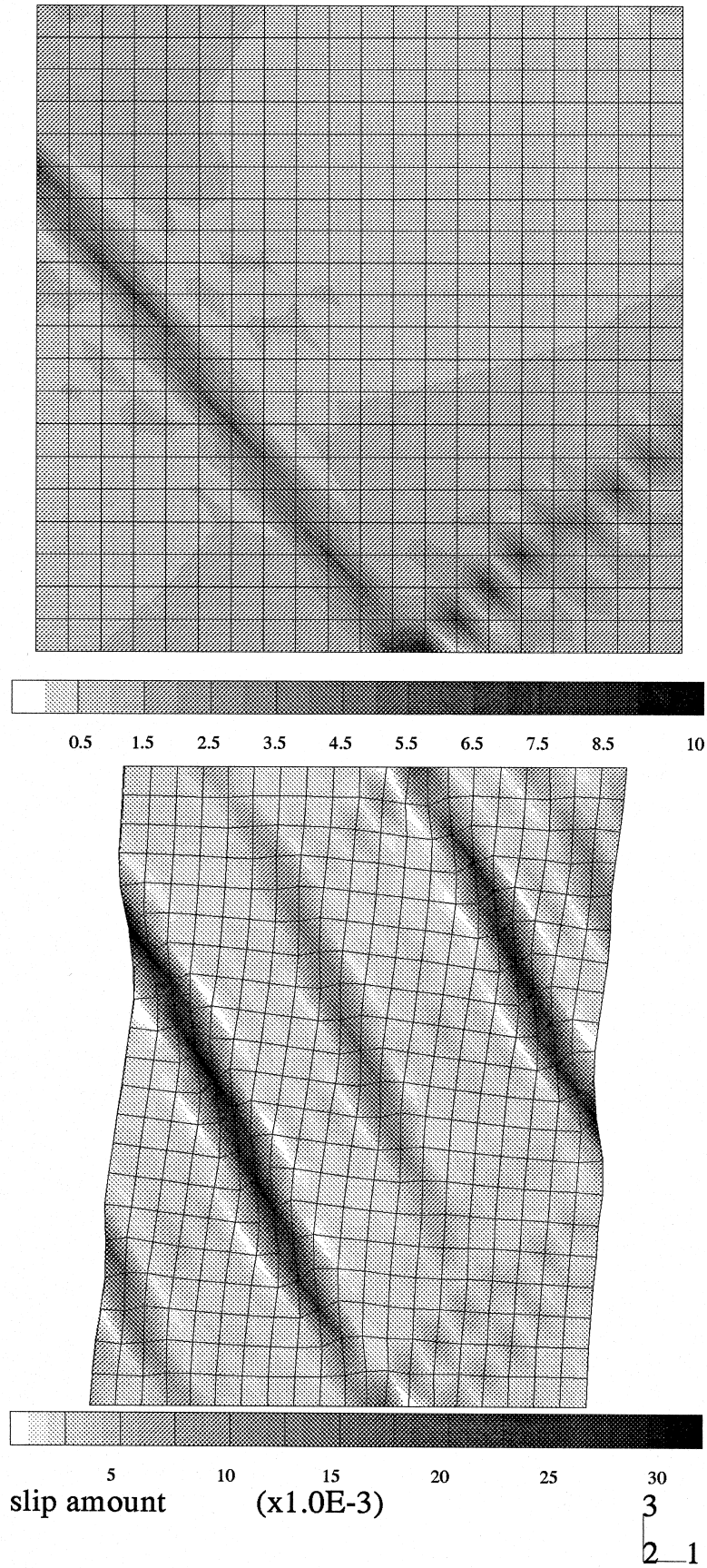


Fig. 10. Strain localization in an elastoviscoplastic Cosserat crystal: slip band formation (above) followed by slip band bundle formation (below).

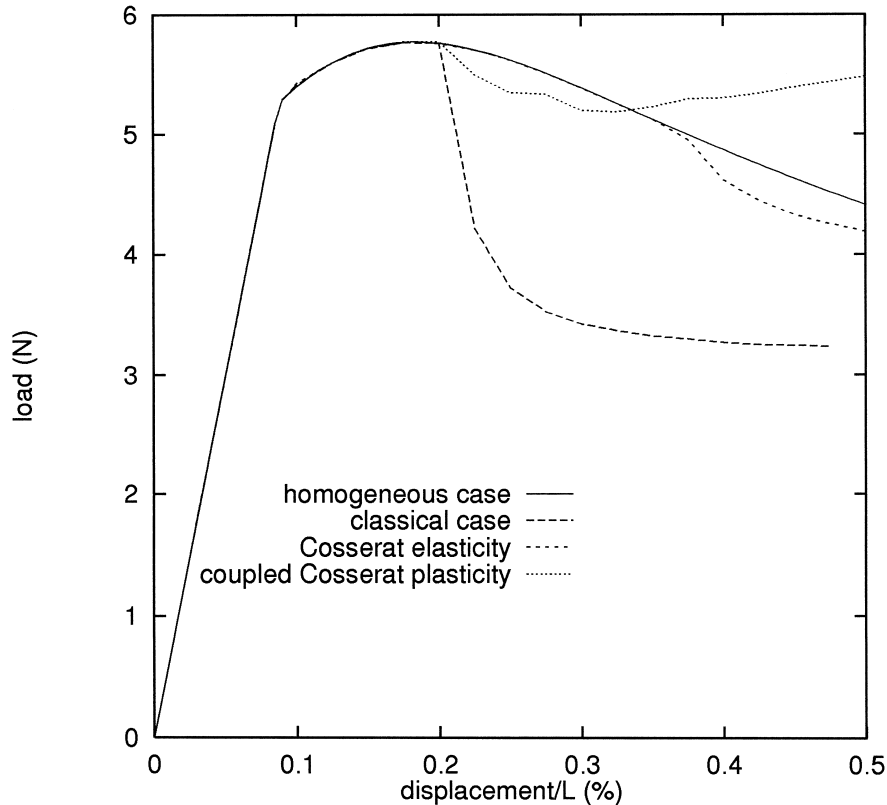


Fig. 11. Load–displacement curves for classical and Cosserat crystal plates oriented for single slip in tension.

crystal plasticity. The coefficients used in this work are only illustrative. The characteristic length l is thought to be the size of the volume element retained for the Cosserat mechanics and depends on the final application one aims at. It must be large enough for this volume element to contain a large amount of dislocations. “Latent” bending tests (bending followed by tension) on single crystals can lead to the determination of H' in equation (33) which accounts for additional resistance to slip due to lattice curvature. This parameter and also H_c (see equation (34)) then control kink band width that may be measured experimentally in some cases.

Acknowledgements—Part of this work has been done within the framework of Brite-Euram project BE-5216 [12]. The author thanks J. Olschewski and R. Sievert from BAM-Berlin where he spent one year. He thanks G. Cailletaud for many discussions and J. Besson for his constant help in FE computing and programming. He is indebted in Gilles Canova for his very stimulating interest in Cosserat crystal modeling before his too abrupt disappearance.

REFERENCES

1. Neuhäuser, H., *Dislocation in Solids*, Vol. 6, ed. F. R. N. Nabarro. Holland Publishing Company, 1983, pp. 319–440.
2. Mader, S., *Z. Phys.*, 1957, **149**, 73.
3. Mader, S. and Seeger, A., *Acta metall.*, 1960, **8**, 513.
4. Jaoul, B., *Etude de la plasticité et application aux métaux*. Dunod, Paris, 1965.
5. Friedel, J., *Dislocations*. Pergamon, 1964.
6. Garstone, J., Honeycombe, R. W. K. and Greetham, G., *Acta metall.*, 1956, **4**, 485.
7. Asaro, R. J. and Rice, J. R., *J. Mech. Phys. Solids*, 1977, **25**, 309.
8. Estrin, Y. and Kubin, L. P., *Acta metall.*, 1986, **34**(12), 2455.
9. Canova, G., Kubin, L. P. and Brechet, Y., in *Large Plastic Deformations*, eds. J. L. Raphanel, C. Teodosiu and F. Sidoroff. Mécamat 91, 1993, pp. 27–38.
10. Besson, J. and Foerch, R., *Comp. Methods Appl. Mech. Eng.*, 1997, **142**, 165.
11. Mandel, J., *Int. J. Solids Struct.*, 1965, **1**, 273.
12. Brite-Euram Project BE 5216, *Development of Microstructural based Viscoplastic Models for an Advanced Design of Single Crystal Hot Section Components*, coordinated by J. Olschewski. BAM, Berlin, 1995.
13. Forest, S. and Cailletaud, G., *Eur. J. Mech. A*, 1995, **14**(5), 747.
14. Hanriot, F., Cailletaud, G. and Rémy, L., *Proc. of Int. Conf. on High Temperature Constitutive Modeling, Theory and Application*, Vol. 1–6. ASME, Atlanta, U.S.A., 1991, pp. 139–150.
15. Rice, J. R., *Theoretical and Applied Mechanics*, ed. W. T. Koiter. North Publishing Company, 1976, pp. 207–220.
16. Peirce, D., Asaro, R. J. and Needleman, A., *Acta metall.*, 1983, **31**(2), 133.
17. Franciosi, P., Berveiller, M. and Zaoui, A., *Acta metall.*, 1980, **28**, 273.
18. Mandel, J., *Int. J. Solids Struct.*, 1973, **9**, 725.

19. Kröner, E., in *Inelastic Behaviour of Solids*, eds. M. F. Kanninen, W. F. Adler, A. R. Rosenfield and R. I. Jaffee. McGraw-Hill, 1969, pp. 137–147.
20. Nye, J. F., *Acta metall.*, 1953, **1**, 153.
21. Ashby, M. F., in *Strengthening Methods in Crystals*, eds. A. Kelly and R. B. Nicholson. Applied Science Publishers, London, 1971, pp. 137–192.
22. Forest, S., Cailletaud, G. and Sievert, R., *Arch. Mech.*, 1997, **49**(4), 705.
23. Teodosiu, C., *Elastic Models of Crystal Defects*. Springer-Verlag, 1982.
24. Walgraef, D. and Aifantis, E. C., *Res. Mech.*, 1988, **23**, 161.
25. Shu, J. Y., Fleck, N. A. and King, W. E., in *MRS Fall Meeting Proc. Symposium W*. 1996, to appear.
26. Smyshlyaev, V. P. and Fleck, N. A., *J. Mech. Phys. Solids*, 1996, **44**(4), 465.
27. Mindlin, R. D. and Eshel, N. N., *Int. J. Solids Struct.*, 1968, **4**, 109.
28. Germain, P., *SIAM J. Appl. Math.*, 1973, **25**(3).
29. Günther, W., *Abh. Braunsch. Wiss. Ges.*, 1958, **10**, 195.
30. Kröner, E., *Int. J. Eng. Sci.*, 1963, **1**, 261.